nature structural & molecular biology

# Structural basis of the specificity of USP18 toward ISG15

Anja Basters[1,5], Paul P Geurink[2,6], Annika Röcker[1,6], Katharina F Witting[2], Roya Tadayon[1,3], Sandra Hess[1], Marta S Semrau[4], Paola Storici[4], Huib Ovaa[2,7], Klaus-Peter Knobeloch[1,7] & Günter Fritz[1,7]



**Protein modification by ubiquitin and ubiquitin-like modifiers (Ubls) is counteracted by ubiquitin proteases and Ubl proteases, collectively termed DUBs. In contrast to other proteases of the ubiquitin-specific protease (USP) family, USP18 shows no reactivity toward ubiquitin but specifically deconjugates the interferon-induced Ubl ISG15. To identify the molecular determinants of this specificity, we solved the crystal structures of mouse USP18 alone and in complex with mouse ISG15. USP18 was crystallized in an open and a closed conformation, thus revealing high flexibility of the enzyme. Structural data, biochemical and mutational analysis showed that only the C-terminal ubiquitin-like domain of ISG15 is recognized and essential for USP18 activity. A critical hydrophobic patch in USP18 interacts with a hydrophobic region unique to ISG15, thus providing evidence that USP18's ISG15 specificity is mediated by a small interaction interface. Our results may provide a structural basis for the development of new drugs modulating ISG15 linkage.**

Post-translational protein modifications by ubiquitin (Ub) and Ubls such as SUMO, NEDD8, FAT10 and interferon-stimulated gene 15 (ISG15) are involved in the regulation of a wide variety of cellular processes including protein stability, DNA repair, cell-cycle control, intracellular trafficking and antiviral defense. ISG15, the first Ubl identified[1], is composed of two Ubl domains connected by a short linker region[2]. Covalent linkage of ISG15 (ISGylation) is mediated by the consecutive action of the E1 activating enzyme Ube1L[3], the E2 conjugating enzyme UbCH8 (refs. 4,5) and several E3 ligases, including mouse HERC6 and human HERC5 (refs. 6–9), which catalyze the conjugation of most substrates in mice and humans, respectively. All components of the ligation process are strongly induced by type I IFN[10].

ISGylation, one of the major antiviral effector systems, is essential to counteract infection by various pathogens including influenza, herpesvirus, norovirus and coronavirus[11,12]. ISGylation occurs at the ribosome in a cotranslational manner, favoring the modification of viral proteins in infected cells[13]. ISGylated capsid proteins fail to assemble properly, thereby inhibiting the propagation of the virus[13]. However, multiple cellular proteins[14,15], including the ubiquitin E2 enzymes Ubc13 (ref. 16) and UbcH6 (ref. 17) as well as the transcription factor IRF3 (refs. 18,19), are modified by ISG15. Moreover, free ISG15 is released from cells and acts in a cytokine-like manner on natural killer cells, thereby stimulating interferon γ (IFN-γ) production[20]. Concordantly, humans with inherited ISG15 deficiency show impaired IFN-γ responses and fail to effectively counteract mycobacterial infection[21]. Beyond the function of ISG15 in immunity, ISGylation is involved in DNA repair[22] and tumorigenesis[23,24].

Analogously to other post-translational control mechanisms, covalent linkage of Ub and Ubls to substrate proteins is a reversible process antagonized by deubiquitinating enzymes and Ubl proteases (DUBs). USPs make up the largest subclass of DUBs[25]. Most of the more than 50 known USPs cleave ubiquitin chains with different types of linkage, and some, such as USP2, USP14 and USP21, have been reported to recognize not only Ub but also ISG15 (refs. 26,27). In contrast to these cross-reactive isopeptidases, USP18 does not deconjugate ubiquitin from target substrates and is the only ISG15-specific protease identified to date[28,29]. However, some reports have indicated that, in a specific context, USP18 is associated with ubiquitin protease activity[30,31]. USP18 cleaves ISG15 from target proteins with high catalytic activity[28] and constitutes the major ISG15 isopeptidase *in vivo*. Accordingly, knock-in mice selectively lacking USP18 enzymatic activity exhibit strongly enhanced and prolonged ISGylation[32]. Intriguingly, enhanced ISGylation in these mice mediates increased resistance against influenza and vaccinia virus infections and diminishes myocarditis after coxsackievirus B3 infection, thus indicating that USP18 protease inhibition is a potential antiviral strategy[33,34]. Irrespective of its enzymatic function, USP18 is a major negative regulator of type I IFN signaling through its interaction with the interferon receptor (IFNAR)[35,36]. Recent studies have shown that depletion of USP18 causes interferonopathies characterized by aberrant microglial activation[35,37]. Furthermore, ISG15 deficiency in humans correlates with destabilization of USP18, thereby enhancing the IFN response[38].

Despite increasing knowledge about these physiological functions of USP18, the molecular structure and determinants of the unique specificity of USP18 toward ISG15 have remained unidentified. The sequence of the catalytic region of USP18 is closely related to that of ubiquitin-deconjugating USPs. In contrast to most other USPs, USP18

[1]Institute of Neuropathology, Faculty of Medicine, University of Freiburg, Freiburg, Germany. [2]Department of Chemical Immunology, Leiden University Medical Center, Leiden, the Netherlands. [3]Hermann-Staudinger Graduate School, University of Freiburg, Freiburg, Germany. [4]Structural Biology Laboratory, Elettra Sincrotrone Trieste S.C.p.A., Trieste, Italy. [5]Present address: Friedrich Miescher Institute for Biomedical Research, Basel, Switzerland. [6]These authors contributed equally to this work. [7]These authors jointly supervised this work. Correspondence should be addressed to G.F. (guenter.fritz@uniklinik-freiburg.de) or K.-P.K. (klaus-peter.knobeloch@uniklinik-freiburg.de).

Received 15 April 2016; accepted 5 January 2017; published online 6 February 2017; doi:10.1038/nsmb.3371

lacks additional typical interaction domains, thus prompting the question of how the unique specificity toward ISG15 is mediated on the molecular level. To gain insights into the mechanism of recognition and catalysis by USP18, we determined structures of mouse USP18 alone and in complex with mouse ISG15, by using X-ray crystallography. Analysis of these structures, biochemical investigations and characterization of several site-specific variants of USP18 provided insights into the molecular determinants of ISG15 recognition and cleavage.

## RESULTS

### Overall structure of USP18

For crystallization experiments, we used the catalytic core of mouse USP18 lacking the N terminus, which has been predicted to be unstructured[28] and is not required for enzymatic activity, ISG15 binding[28] or interaction with IFNAR[36]. The unbound USP18 protein crystallized as thin needles that diffracted to a resolution of 2.8 Å (**Table 1**). There were two molecules in the asymmetric unit, forming an extended crystal contact covering a surface area of 900 Å$^2$. A single $Zn^{2+}$ ion stabilizes the crystal contact (**Supplementary Fig. 1a**) and is coordinated by residues His334 and Cys336 of both molecules (**Supplementary Fig. 1c**).

The USP18 structure adopts the typical fold of the catalytic core of USPs, resembling a right hand (**Fig. 1** and **Supplementary Fig. 2**). The three major domains are therefore termed the finger, palm and thumb domains[39] (**Supplementary Fig. 2**). The finger domain encompasses a $Zn^{2+}$ coordinated by four cysteine residues stabilizing the extended loop of the finger domain (**Supplementary Fig. 1a**,**b**).

### USP18 adopts two conformations in the crystal

Structural alignment of the two different USP18 molecules present in the asymmetric unit revealed some marked differences. Whereas the palm and thumb domains of the two chains A and B align well, the orientation of the finger domain differs in each molecule. The finger domain of chain B exerts a closing movement toward the thumb domain, reorienting β-sheets 4 and 5 and the connecting loop by 10 Å (**Fig. 1**). Furthermore, the loop located between residues 126 and 136 exhibits major differences. This loop corresponds to the previously described switching loop of USP7 and has been shown to influence the catalytic activity[40]. Whereas in one USP18 molecule (chain B), this loop exhibits no secondary structure, residues 131–135 of the second molecule (chain A) fold into a short α-helix. Minor differences were observed, for example, for a loop comprising residues 307–314 and corresponding to the so-called blocking loop 2, which has been described in several USPs, such as USP14 (ref. 41), USP8 (ref. 42) and USP7 (ref. 43). With respect to the USP18 finger domain, the two conformations were assigned to an 'open' and a 'closed' state.

The structure of the USP18–ISG15 complex, described below, revealed that the closed state of USP18 is not compatible with ISG15 binding. Residues Cys61, His314 and Asn331 form the catalytic triad of USP18. The distances between these residues within the two molecules of unbound USP18 are very similar: the Cys61 Sγ and the His314 Nδ1 atom are separated by 4.0–4.2 Å, and the carbonyl group of the Asn331 side chain resides at a distance of 3.5–3.7 Å from the Nε2 atom of His314 (**Fig. 1c**,**d** and **Supplementary Fig. 3a**,**b**). The observed distances suggest that the catalytic triad is not in catalytic configuration in unbound USP18. In summary, the USP18 molecules in the asymmetric unit correspond to two different states that are both enzymatically inactive.

### Structure of the USP18–ISG15 complex

The covalent complex of mouse USP18 with mouse ISG15 was prepared with ISG15 modified with a C-terminal propargylamide (PA) reactive group (ISG15-PA)[44]. The crystals diffracted to a resolution of 3.0 Å (**Table 1**). There were two USP18–ISG15 complexes in the asymmetric unit. In the complex, in contrast to the uncomplexed enzyme, the USP18 molecules adopt virtually identical conformations with an r.m.s. deviation (r.m.s.d.) of 0.4 Å over 300 Cα positions (**Fig. 1**). These observations suggest that unbound USP18 exhibits pronounced conformational flexibility but is arrested in a distinct conformation after ISG15 is bound.

**Table 1 Data collection and refinement statistics**

| | USP18 (PDB 5CHT) | USP18–ISG15 (PDB 5CHV) |
|---|---|---|
| **Data collection** | | |
| Space group | $P2_12_12_1$ | $P2_12_12_1$ |
| Cell dimensions | | |
| *a*, *b*, *c* (Å) | 53.96, 89.75, 149.40 | 64.04, 72.80, 217.26 |
| *α*, *β*, *γ* (°) | 90, 90, 90 | 90, 90, 90 |
| Resolution (Å) | 28–2.8 (2.95–2.8)[a] | 37–3.0 (3.16–3.0) |
| $R_{merge}$ (%) | 30.1 (277.1) | 62.7 (293.4) |
| $R_{pim}$ (%) | 30.1 (134.5) | 18.0 (84.4) |
| $I/\sigma(I)$ | 6.29 (0.79) | 3.53 (0.86) |
| $CC_{1/2}$ | 98.3 (23.9) | 97.1 (34.8) |
| Completeness (%) | 99.7 (99.9) | 99.9 (99.9) |
| Redundancy | 4.86 (4.95) | 13.0 (12.9) |
| **Refinement** | | |
| Resolution (Å) | 28–2.8 | 37–3.0 |
| No. reflections | 18,487 | 20,936 |
| $R_{work}$ / $R_{free}$ (%) | 22.5 / 28.3 (39.0 / 40.8) | 22.5 / 28.6 (32.6 / 36.9) |
| No. atoms | 4,943 | 7,445 |
| Protein | 4,885 | 7,426 |
| Ion | 3 | 14 |
| Water | 55 | 5 |
| *B* factors | | |
| Protein | 74.1 | 59.3 |
| Ion | 78.4 | 66.0 |
| Water | 51.8 | 18.2 |
| R.m.s. deviations | | |
| Bond lengths (Å) | 0.009 | 0.003 |
| Bond angles (°) | 1.059 | 0.736 |

Data were collected from one crystal per condition. [a]Values in parentheses are for the highest-resolution shell.

ISG15 consists of two Ubl domains connected by a flexible linker region. In both complexes, ISG15 interacts extensively via its C-terminal Ubl domain with the palm and thumb domain of USP18 (**Fig. 2a**), covering an area of 1,870 Å$^2$. This area is similar in size to the contact area formed between Ub and USP7 (ref. 39) or Ub and USP21 (ref. 27). The C-terminal tail of ISG15 containing the LRLRGG motif also present in ubiquitin binds the active site cleft of USP18 (**Fig. 2a** and **Supplementary Fig. 3c**,**d**).

An extensive network of hydrogen bonds mediates the interaction between ISG15 and USP18. In addition, a hydrophobic pocket of the USP18 palm domain accommodates the residues Leu150 and Leu152 of ISG15. This mode of binding closely resembles the interaction of ubiquitin with other USPs such as USP7 (ref. 39).

### The ISG15 C-terminal Ubl is necessary and sufficient for USP18 binding

The comparison of both USP18–ISG15 complexes in the asymmetric unit revealed that the C-terminal Ubl domains of ISG15 align with high similarity (r.m.s.d. of 0.5 Å over 73 Cα positions). In contrast,

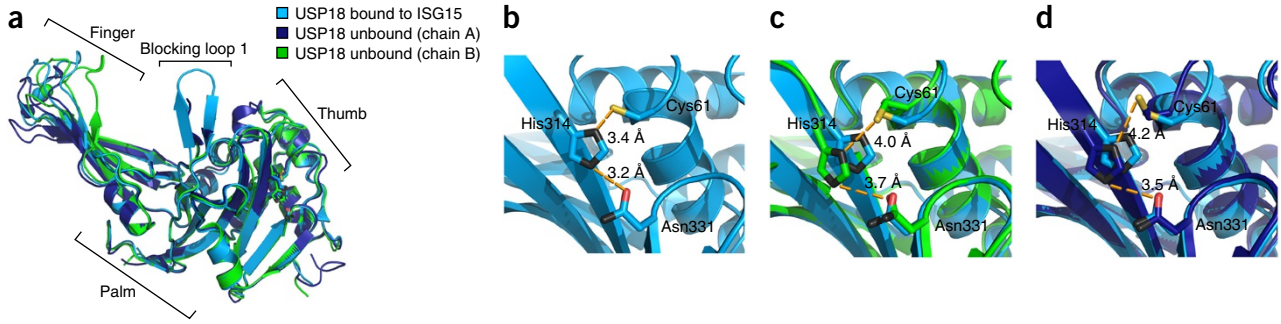


**Figure 1** Structure of USP18 in the unbound and ISG15-bound state. (**a**) USP18 crystallized with two molecules in the asymmetric unit. Superposition of the two molecules in the asymmetric unit (dark blue, chain A; green, chain B). For comparison, ISG15-bound USP18 (light blue) is structurally aligned. The $Zn^{2+}$ ions in the finger domain are shown as spheres and illustrate the extent of the movement. Residues 255–267 corresponding to blocking loop 1 are disordered in unbound USP18 and are not resolved in the electron density, whereas they form a short antiparallel β-sheet in ISG15-bound USP18. (**b**–**d**) Close-up views of the catalytic triad in ISG15-bound (**b**) and unbound (**c**,**d**) USP18. In all structures of USP18, the residues Cys61, His314 and Asn331, which form the catalytic triad, are in proximity. (**b**) Only in ISG15-bound USP18 do the side chains of the three residues exhibit the correct orientation and distances to stabilize a thiolate state of the Sγ of Cys61. (**c**,**d**) In both molecules of unbound USP18, the imidazole of His314 is slightly shifted away from Cys61, thereby weakening the interaction of the two side chains.

the N-terminal domain shows no or only marginal interaction with USP18, and its orientation markedly differs between both complexes (**Fig. 2a**): in one complex, the N-terminal Ubl domain approaches the thumb domain, with the closest distance between Cα positions of 8 Å (**Fig. 2a**), whereas in the second complex, the N-terminal domain resides at a distance of 18 Å from USP18 (**Fig. 2a**). This conformational difference corresponds to a rotational movement of approximately 10° around the flexible linker region of ISG15.

Together, the structural data suggest that only the C-terminal domain of ISG15 is critical for interaction with USP18. This result is in contrast to the structures of di-Ub in complex with USP21 (ref. 27) or with SARS coronavirus PLpro[45], in which both domains of di-Ub show noticeable contacts with the protease. On the basis of the structure of USP21 in complex with di-Ub, USP18 has been suggested to bind ISG15 in a similar manner. To validate our structural observations, we tested the reactivity of USP18 toward the isolated C-terminal Ubl domain of ISG15 (ct-ISG15) compared with full-length ISG15 (both constructs were modified with a PA group as an active site probe). Both full-length ISG15-PA and ct-ISG15-PA readily reacted with the active site cysteine of USP18 and formed a covalent complex. In contrast, no binding of USP18 to the respective Ub probe[44] was observed (**Fig. 2b**). Likewise, the kinetic analysis of USP18 reactivity toward a fluorescent ct-ISG15-FP substrate revealed highly efficient cleavage (**Table 2** and **Supplementary Fig. 4a**). Moreover, USP18 cleaved ct-ISG15 as effectively as it cleaved full-length ISG15 from cellular substrates (**Fig. 2c**). Thus, our results demonstrate that only the C-terminal Ubl domain of ISG15 is essential and sufficient for USP18 binding and activity.

### ISG15 binding induces conformational changes in USP18

Alignment of the unbound USP18 molecules with the ISG15-bound USP18 revealed substantial structural differences. The most obvious changes occur at the finger domain, which, after binding to ISG15, adopts an orientation intermediate between the two different conformations of unbound USP18 (**Fig. 1a**). Moreover, the region comprising residues 255–267, which is disordered in unbound USP18, folds into a short stable antiparallel β-sheet (**Fig. 3a**). This part corresponds to blocking loop 1 in other USPs, such as USP14 (ref. 41).

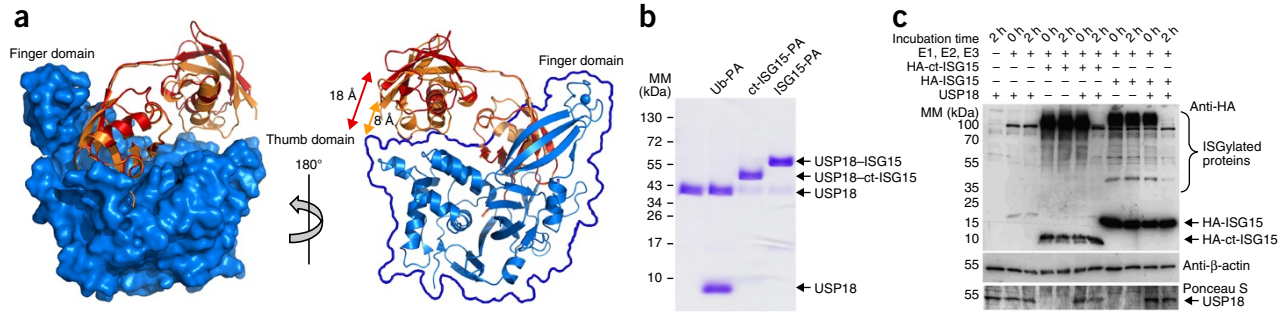


**Figure 2** The C-terminal Ubl domain of ISG15 is sufficient for USP18 binding and activity. (**a**) Structural alignment of both USP18–ISG15 complexes present in the asymmetric unit. For clarity, only one USP18 molecule (blue) is shown. Left, surface representation of USP18 (blue) with ISG15 aligned from both complexes (red and orange). Right, the molecules are rotated by 180°. USP18 is shown as a cartoon with an outline of the surface. The C-terminal Ubl domain of ISG15 is embedded between the finger and the thumb domains. In contrast, the N-terminal Ubl domain of ISG15 exhibits no contacts to USP18. In both complexes, the N-terminal domain adopts a different position with regard to the C-terminal domain and is located 8 Å or 18 Å from the USP18 thumb domain (distance between the Cα atoms of ISG15 Ser22 and USP18 Glu91). (**b**) Coomassie-stained SDS–PAGE showing that USP18 reacts with full-length ISG15 and the C-terminal domain of ISG15 (ct-ISG15) with the same efficiency. The reaction products of stoichiometric amounts of USP18 with full-length ISG15-PA, ct-ISG15-PA or ubiquitin-PA (Ub-PA) were visualized as a shift in molecular mass (MM). (**c**) Immunoblot showing cleavage of ct-ISG15 from cellular substrates by recombinant USP18. Cell lysates with cellular substrates modified by hemagglutinin (HA)-tagged ct-ISG15 or HA-tagged-full-length ISG15 were incubated with recombinant USP18. Top, deconjugation of ISG15 from cellular proteins, as monitored with an anti-HA antibody. Middle, β-actin was used as a loading control. Bottom, Ponceau S staining shows the presence of USP18.

**Table 2 Kinetic parameters of mouse USP18 and variants**

| Protein | Reagent | $K_m$ (μM) | $k_{cat}$ ($s^{-1}$) |
|---|---|---|---|
| USP18* | ISG15-FP | 4.8 ± 0.3 | 0.23 ± 0.3 |
| $USP18^{IBB\text{-}1\text{-}USP7}$** | ISG15-FP | NA** | $1.2 \times 10^{-4} \pm 0.6 \times 10^{-4}$** |
| $USP18^{IBB\text{-}2\text{-}USP7}$ | ISG15-FP | 39 ± 11 | 0.15 ± 0.04 |
| $USP18^{IBB\text{-}1\text{-}USP7\text{–}IBB\text{-}2\text{-}USP7}$ | ISG15-FP | NA | NA |
| USP18 | ct-ISG15-FP | 0.48 ± 0.03 | 0.07 ± 0.01 |

*Values from ref. 28. **No saturation was observed at the concentrations that could be used in the assay. The highest activity observed is reported. No $K_m$ value could be extracted from the data. NA, not applicable. Errors represent error of fit on the basis of 12 different substrate concentrations with 3 replicates.

Another major structural change occurs in the switching loop. In ISG15-bound USP18, residues 129–135 of the thumb domain form an extended loop. This conformation enables access of the C-terminal LRLRGG tail of ISG15 into the catalytic cleft. In contrast, in unbound USP18, residues 131–135 fold into a short α-helix. A structural overlay of unbound USP18 and the USP18–ISG15 complex reveals that residues Arg151 and Arg153 of the LRLRGG motif clash with this short α-helix of unbound USP18 (**Fig. 3b**). Therefore, the α-helix must unwind, and the loop must change its conformation to allow for ISG15 binding. Finally, the catalytic triad in ISG15-bound USP18 is formed by small movements of all three involved residues (His314, Asn331 and Cys61) (**Fig. 1b–d**).

### Comparison with ubiquitin-binding USPs

The overall structures of USP–Ub complexes and the USP18–ISG15 complex are markedly similar (**Fig. 4a**,**b**), and, as shown here, only the C-terminal Ubl domain of ISG15 is required for binding. This result prompts questions how the exceptional specificity of USP18 is achieved and which particular residues are involved. To identify critical residues, we performed a Dali search[46] with the structure of ISG15-bound USP18, defining USP2, USP4, USP5, USP7, USP8, USP14 and USP21 as the closest homologs. These proteases align with USP18 with r.m.s.d. values between 1.8 Å and 2.7 Å. The highest similarity is shared between USP18 and USP7 (r.m.s.d. of 1.8 Å over 290 Cα). Although the SARS coronavirus PLpro shows high deISGylation activity[45], the structural alignment reveals only an r.m.s.d. of 3.5 Å over 196 Cα.

Intriguingly, the residues required for recognition of the C-terminal tail of ISG15 or Ub are strictly conserved among USP18, ubiquitin-processing USPs and the SARS CoV enzyme PLpro. Thus, other areas of USP18 must confer the specificity for ISG15. A structure-based sequence alignment of these proteases revealed a number of residues that are important for ISG15 binding yet are unique to USP18 (**Supplementary Note**). Two areas in the USP18-binding surface were identified as candidates that may confer specificity toward ISG15. The first area comprises residues Ala138, Leu142, Ser192 and His251 of USP18, which form a contiguous patch (**Fig. 4a** and **Supplementary Note**). The second area encompasses residues 256–263, located in blocking loop 1 (**Fig. 4a** and **Supplementary Note**). We defined these areas as ISG15-binding box 1 and box 2 (IBB-1 and IBB-2, respectively).

### IBB-1 and IBB-2

IBB-1 provides exclusively hydrophobic contacts with ISG15. The side chains of His149 and Trp121 in ISG15 are in proximity, forming a π-π contact that stabilizes the orientation of these residues and forms a hydrophobic bulb. In USP18, residues His251, Ala138 and Leu142 are part of a hydrophobic pocket that perfectly accommodates the hydrophobic bulb of ISG15 (**Fig. 4c**). This characteristic

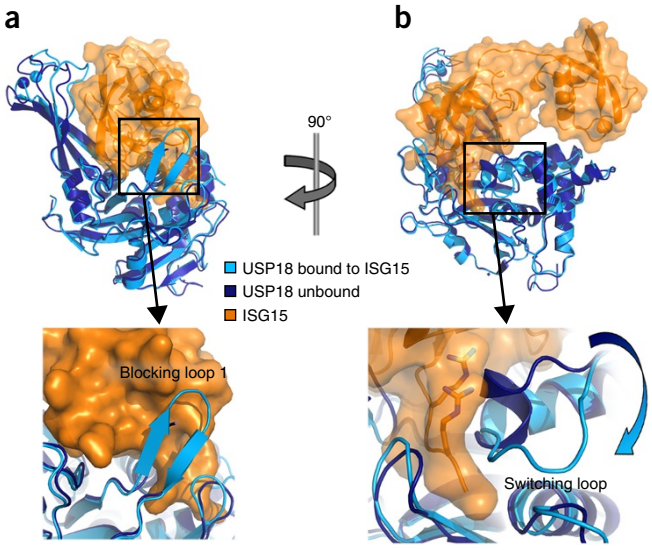


**Figure 3** Conformational changes in USP18 after ISG15 binding. Structural alignment of USP18 (light blue) bound to ISG15 (orange) and unbound USP18 (dark blue), revealing a conformational change in the finger domain and in the blocking and switching loops. (**a**) Residues 255–267 (blocking loop 1), which are unordered in unbound USP18, fold into a short β-sheet that interacts with ISG15. (**b**) The switching loop connects helix 4 and helix 5 of the thumb domain and comprises residues 129–135. In unbound USP18, residues 131–135 fold into a short α-helix that blocks the access of the C-terminal LRLRGG motif of ISG15 to the catalytic site of USP18. In ISG15-bound USP18, the α-helix unwinds, and the entire loop comprising these residues is displaced.

hydrophobic contact is further stabilized by the side chain of Pro128 of ISG15 and Leu142 of USP18 (**Fig. 4c**). The corresponding regions of USP7 largely differ from USP18. In particular, the residues in USP7 corresponding to IBB-1 are more bulky and polar. Ser192, His251 and Ala138 of USP18 are all substituted by glutamine residues in USP7. The hydrophobic Leu142 is replaced by an arginine. In particular, replacement of Ala138 in USP18 by a polar residue in other USPs might block the access of the bulky and hydrophobic Trp121 side chain of ISG15 (**Fig. 4d**). In contrast to IBB-1, IBB-2, located on blocking loop 1, mediates hydrogen-bond interactions with ISG15 (**Fig. 4e**). The corresponding blocking loop in USP7 is extended by two residues and adopts a conformation incompatible with ISG15 or ubiquitin binding. No hydrogen bonds are formed between USP7 and ubiquitin in this region (**Fig. 4f**).

To evaluate the roles of IBB-1 and IBB-2, we created USP18 variants bearing the respective residues of USP7. In $USP18^{IBB\text{-}1\text{-}USP7}$, residues Ala138, Leu142, His251 and Ser192 of IBB-1 were replaced with those of USP7; in $USP18^{IBB\text{-}2\text{-}USP7}$, the blocking loop 1 of USP7 was inserted; and in $USP18^{IBB\text{-}1\text{-}USP7\text{–}IBB\text{-}2\text{-}USP7}$, both modifications were combined. Likewise, we generated an ISG15 variant bearing an arginine residue instead of Trp121 (ISG15 W121R), as well as a variant in which Trp121, Pro128 and His149 of ISG15 were changed to the corresponding residues of ubiquitin (ISG15 W121R P128G H149V). The interaction of mouse USP18 with ISG15 and several variants was analyzed by surface plasmon resonance (SPR; binding curves and parameters in **Supplementary Fig. 5**). ISG15 bound to immobilized USP18 with a high affinity characterized by a fast association and dissociation phase. The $K_d$ of 1.49 ± 0.03 μM (mean ± s.d.) is in good agreement with the $K_d$ of 1.3 ± 0.2 μM determined previously by microscale thermophoresis[28]. Changing the residues in IBB-1 to the corresponding residues of USP7 (variant $USP18^{IBB\text{-}1\text{-}USP7}$), or making

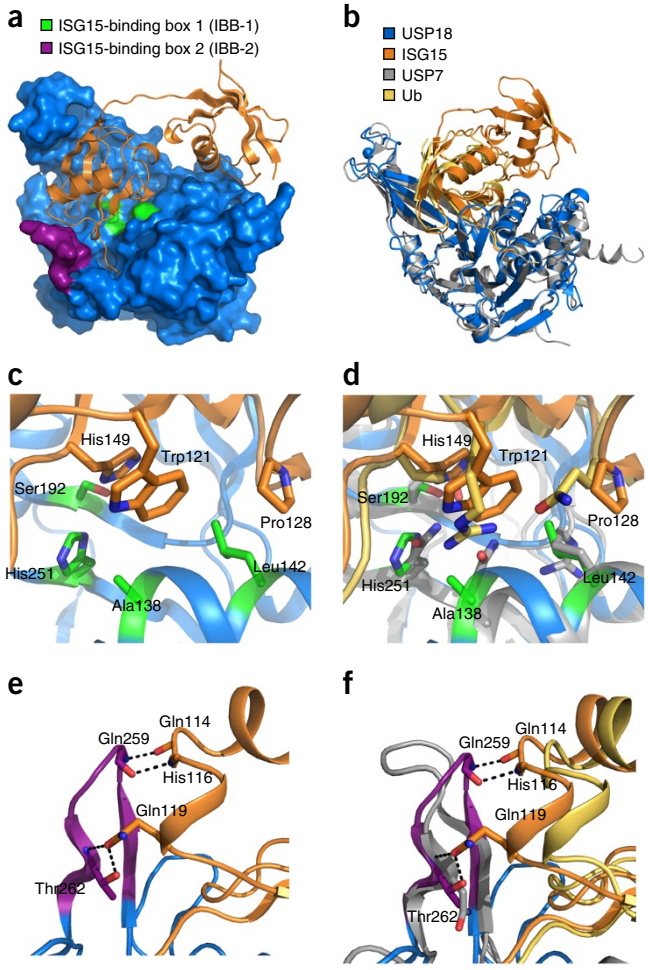


**Figure 4** ISG15-binding boxes 1 and 2 in USP18. (**a**) Structure of the USP18–ISG15 complex. Blue, USP18; orange, ISG15; green, IBB-1 of USP18; purple, IBB-2 of USP18. (**b**) Structural alignment of the USP18–ISG15 complex with the USP7–Ub complex (PDB 1NBF)[39]. Blue, USP18; orange, ISG15; gray, USP7; yellow, Ub. The orientation of Ub bound to USP7 closely resembles the orientation of the ISG15 C-terminal domain in the USP18–ISG15 complex. (**c**) Close-up view of IBB-1. The residues of USP18 forming IBB-1 are shown in green and form a hydrophobic pocket that accommodates the bulky aromatic side chain of Trp121 from ISG15 (orange). (**d**) Superposition of IBB-1 with the respective region of the USP7–Ub complex. The labeling refers to residues in USP18 and ISG15. The interaction between USP18 and ISG15 is mediated by hydrophobic residues, whereas USP7 and ubiquitin display polar residues in this region. (**e**) Close-up view of IBB-2 (purple), showing several residues of a short antiparallel β-sheet of USP18 forming hydrogen bonds (dotted lines) with ISG15. For clarity, the side chains of the interacting residues are omitted. (**f**) Superposition of IBB-2 with the respective region of the USP7–Ub complex. The distances between ubiquitin and USP7 are larger than those in the USP18–ISG15 complex.

similar changes in IBB-2 (variant USP18$^{IBB\text{-}2\text{-}USP7}$), resulted in a clear decrease in affinity toward ISG15. A more drastic decrease in affinity was observed for USP18$^{IBB\text{-}1\text{-}USP7\text{–}IBB\text{-}2\text{-}USP7}$, which contained both changes. To validate these results, we also analyzed variants of ISG15 with changes in the residues interacting with IBB-1 of USP18. The exchange of Trp121 in ISG15 to the corresponding arginine of Ub (variant ISG15 W121R) caused a clear decrease in affinity, and mutation of all three interacting residues, Trp121, Pro128 and His149 (variant ISG15 W121R P128G H149V), almost completely abolished the interaction with USP18. Likewise, the observed binding ratio of ISG15 per immobilized USP18 decreased to 0.4 when Trp121 was mutated, and no clear stoichiometry of binding could be obtained for the variant ISG15 W121R P128G H149V, thus indicating that the observed binding might be due to a residual unspecific interaction. The observations for the ISG15 variants corroborated the structural data showing that IBB-1 is an important determinant of the interaction between USP18 and ISG15.

To analyze the effects of changes in IBB-1 and IBB-2 on the catalytic activity of the enzyme, all three variants of mouse USP18 were tested for covalent adduct formation with ISG15-PA, ct-ISG15-PA and Ub-PA[44]. Wild-type (WT) USP18 reacted readily with ISG15-PA and ct-ISG15-PA within 1 min. In contrast, USP18$^{IBB\text{-}1\text{-}USP7}$ formed no adduct, even after 5 min. The covalent adduct was observed only after prolonged incubation (**Fig. 5a**). USP18$^{IBB\text{-}2\text{-}USP7}$ reacted almost as rapidly as WT, but completion of the reaction was impaired, as indicated by the presence of unreacted USP18. Strikingly, mutation of both IBBs in USP18$^{IBB\text{-}1\text{-}USP7\text{–}IBB\text{-}2\text{-}USP7}$ completely abolished covalent-complex formation (**Fig. 5a**). Notably, neither WT USP18 nor the USP18 variants reacted with Ub-PA, even after prolonged incubation (**Supplementary Fig. 6a**). As shown by multiple sequence alignments, IBB-1 and IBB-2 are well conserved among mammalians (**Supplementary Fig. 7**). To evaluate whether human USP18 recognizes the ISG15-like mouse USP18, we built a 3D model of the human USP18–ISG15 complex on the basis of the structure of the mouse USP18–ISG15 complex. As expected, the interaction surfaces are complementary, and the model suggests that IBB-1 of human USP18 is crucial for reactivity (data not shown). To evaluate these observations, we expressed and purified human USP18 and generated a human ISG15-PA probe. Because the interaction surfaces in the USP18–ISG15 complex are well conserved between human and mouse proteins, we tested whether the ISG15-PA active site probes would label USP18 across species. As predicted by the model, human USP18 reacted readily with mouse ISG15-PA and vice versa (**Supplementary Fig. 6b**).

Next, we expressed human USP18 and USP18 variants carrying mutations for the active site cysteine, IBB-1 or IBB-2 in HEK 293T cells and tested those for reactivity (**Supplementary Fig. 6c**,**d**). WT mouse and human USP18 were readily labeled by mouse and human ISG15-PA, whereas the variants of USP18 lacking the active site cysteine (mouse US18 C61A and human USP18 C64A) showed no reactivity (**Supplementary Fig. 6c**,**d**). Changing the residues of IBB-1 in human USP18 to the corresponding residues of USP7 abolished the reactivity of human USP18 toward human ISG15-PA. This result was fully consistent with the results obtained for the mouse enzyme. Changing the residues of IBB-2 in human USP18 had no noticeable effect, thus corroborating the results obtained for mouse USP18. Because we introduced the residues of ubiquitin-cleaving USP7, we tested whether human USP18 WT or the different human USP18 variants were reactive toward Ub-PA. Neither human USP18 nor the variants were labeled by Ub-PA (**Supplementary Fig. 6d**).

To further characterize the importance of IBB-1 and IBB-2, we tested the three mouse USP18 variants for ISG15 deconjugation activity by using ISG15-FP[28] and ct-ISG15-FP as substrates in a fluorescence polarization assay. The kinetic analysis corroborated the previous results (**Fig. 5b**). For USP18$^{IBB\text{-}1\text{-}USP7}$, only minor residual catalytic activity was observed (0.5% of WT activity), whereas USP18$^{IBB\text{-}2\text{-}USP7}$ still cleaved the model substrate but did so with a lower efficiency than that of USP18 WT (65% of WT activity). USP18$^{IBB\text{-}1\text{-}USP7\text{–}IBB\text{-}2\text{-}USP7}$ entirely lost enzymatic activity (kinetic parameters in **Table 2**). Neither WT USP18 nor the USP18 variants showed activity toward the Ub-FP substrate (**Supplementary Fig. 4b**–**e**).

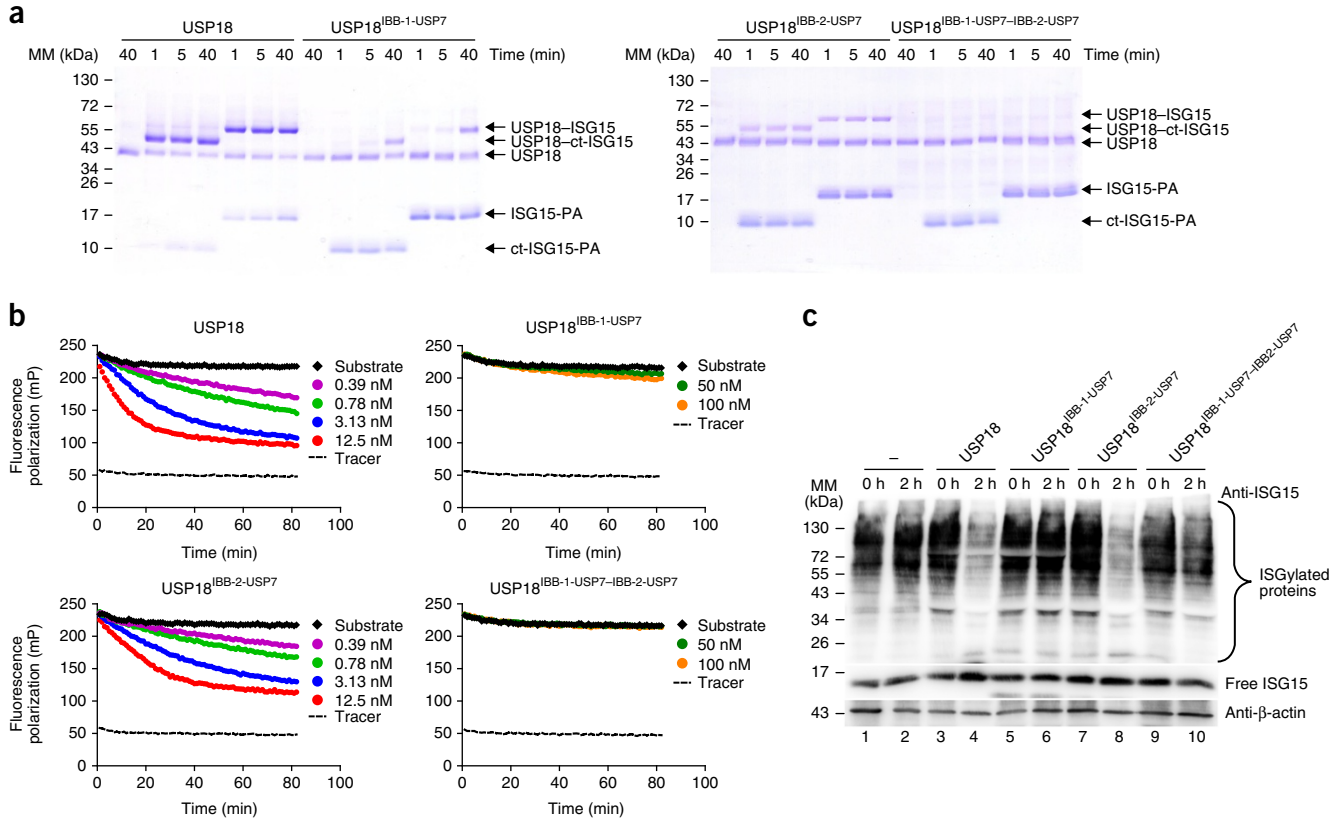


**Figure 5** IBB-1 but not IBB-2 is critical for USP18 activity. (**a**) Coomassie blue–stained SDS–PAGE showing the reactivity of USP18 WT and variants toward ISG15-PA and ct-ISG15-PA probes after incubation for the indicated times. The figure shown is representative of three independent experiments. (**b**) Catalytic activity of USP18 WT and variants toward the ISG15-FP substrate, as shown by substrate cleavage, monitored on the basis of the change in fluorescence polarization (in millipolarization units (mP)). Different amounts of USP18 proteins were incubated with ISG15-FP. (**c**) Immunoblot analyses showing deISGylation of endogenous substrates by USP18 WT or variants. ISG15 cleavage by USP18 was monitored with an antibody directed against ISG15.

Next, we addressed the contributions of IBB-1 and IBB-2 to the recognition of endogenous cellular substrates of USP18. USP18-deficient cells were stimulated with interferon β to induce ISGylation of cellular proteins serving as substrates for recombinant USP18. As expected, WT USP18 added to cell lysates readily deconjugated ISG15 (**Fig. 5c**, lane 4). USP18$^{IBB\text{-}1\text{-}USP7}$ showed no apparent cleavage (**Fig. 5c**, lane 6), whereas USP18$^{IBB\text{-}2\text{-}USP7}$ still cleaved ISG15 conjugates (**Fig. 5c**, lane 8). In agreement with the results from all previous experiments, USP18$^{IBB\text{-}1\text{-}USP7\text{–}IBB\text{-}2\text{-}USP7}$ did not cleave endogenous substrates. In summary, our results showed that proper accommodation of the ISG15 hydrophobic patch is critical for both human and mouse USP18 activity, because even minor changes in this region had marked effects on enzyme activity.

### The hydrophobic nature of IBB-1 is critical for ISG15 specificity

Multiple sequence alignments of USP18 show that the hydrophobic character of IBB-1 is highly conserved among mammals and marsupialia (**Supplementary Fig. 7**). Likewise, the corresponding counterpart in ISG15, which carries the bulky tryptophan protruding from the surface, is also highly conserved (**Supplementary Fig. 8**). Thus, the hydrophobic interaction described here appears to be strictly conserved among different species. In particular, IBB-1 of USP18 and the hydrophobic patch of ISG15 are among the most conserved regions between these proteins. A similar degree of conservation was observed for only the catalytic cleft of USP18 and the C-terminal tail of ISG15 (**Supplementary Figs. 7b** and **8b**). In contrast, instead of carrying the two hydrophobic residues Ala138 and Leu142 (*Mus musculus* numbering), fish USP18 carries an aspartate and a histidine residue at the corresponding positions (**Supplementary Fig. 7a**). Most interestingly, in fish ISG15, these variations are compensated by an exchange of the hydrophobic Trp121 and Pro128 (*M. musculus* numbering) to the polar residues arginine and glutamine, respectively (**Supplementary Fig. 8a**). A molecular model of a USP18–ISG15 complex bearing these mutations suggests that the side chains of these polar residues can form several hydrogen bonds. This type of interaction is reminiscent of the interactions between other USPs and ubiquitin. Thus, we speculated that fish USP18 might not be restricted to ISG15 but may also be able to recognize ubiquitin. To test this hypothesis, we expressed USP18 from *Danio rerio* in HEK 293T cells and analyzed the cell lysates for reactivity with ISG15- and Ub-reactive probes (**Fig. 6a**). USP18 from *D. rerio* reacted readily with mouse ISG15-PA (**Fig. 6b**). Most interestingly, USP18 from *D. rerio* reacted with not only ISG15-PA but also mammalian Ub-PA, whereas mouse USP18 showed no cross-reactivity with Ub (**Fig. 6c**), as previously reported[28]. Although the portion of covalent modification of USP18 from *D. rerio* with Ub appeared to be less than that with ISG15, the modification was clearly visible and was not observed when the active site cysteine was mutated to alanine (**Fig. 6c**). These data further support that the IBB-1 region is critical for ISG15 specificity.

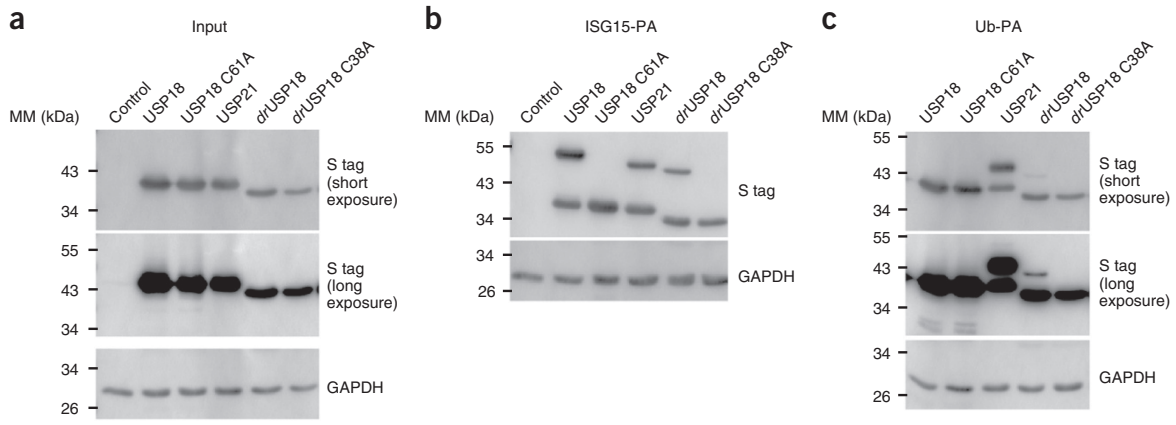


**Figure 6** Zebrafish USP18 recognizes ISG15 and ubiquitin. (**a**) Immunoblot of lysates from HEK 293T cells transfected with S-tagged versions of mouse USP18 (mUSP18), mouse USP18 with the active site cysteine replaced by alanine (mUSP18 C61A), human USP21 (hUSP21), zebrafish USP18 (*dr*USP18) and zebrafish USP18 with the active site cysteine replaced by an alanine (*dr*USP18 C38A) or from untransfected cells (control). Protein expression was visualized with an antibody directed against the S tag. (**b**) Immunoblot of lysates from cells transfected with the indicated expression constructs, incubated with the active site–directed probe ISG15-PA. Complex formation was monitored on the basis of a size shift detected with an anti-S-tag antibody. (**c**) Immunoblot analyses of protein lysates from cells transfected with the indicated expression constructs, incubated with the active site–directed probe Ub-PA. Complex formation was monitored on the basis of a size shift detected with an anti-S-tag antibody. USP21 is cross-reactive for ISG15, and ubiquitin served as a positive control for Ub binding. Results shown in **a**–**c** are representative of three independent experiments.

## DISCUSSION

Most members of the USP family of DUBs cleave different types of ubiquitin chains from substrates. In addition, some USPs show cross-reactivity toward ISG15 (ref. 26). To ensure specific functions of the different USPs, most enzymes of the USP family have additional large domains mediating interaction with other protein complexes[47] or specific organelles[48], or they show temporal distributions[49]. In contrast, USP18 is a notably small member, which comprises only the USP core domain. Nevertheless, USP18 is specific for ISG15 and is not cross-reactive toward ubiquitin or any other member of the Ubl family[28,29]. Thus, the unique specificity must arise entirely from the USP core domain itself. Models based on structures of the isopeptidases USP21 (ref. 27) and the viral SARS CoV PLpro[50], both of which cleave ISG15 and ubiquitin, suggest that USP18 might recognize both Ubl domains of ISG15. In the USP21–di-Ub complex, the N-terminal Ub domain is in contact with the finger domain. In the SARS CoV PLpro, binding of the N-terminal Ubl domain to the thumb domain has been observed. However, no structure of a complex of full-length ISG15 with an ISG15 protease is currently available. Our analysis demonstrates that only the C-terminal Ubl domain of ISG15 is sufficient for USP18 binding and activity. Moreover, we identified the structural determinants essential for the extraordinary substrate specificity of USP18. We mapped two regions, IBB-1 and IBB-2, which are unique to USP18 and recognize regions that are present in the C-terminal Ubl domain of ISG15 but are absent in ubiquitin. Analysis of site-specific variants showed that IBB-1 is the major determinant of ISG15 cleavage, whereas IBB-2 has only minor contributions. This result is also reflected in the conservation of IBB-1 across different species. Whereas these residues are strictly conserved in IBB-1 in mammals, fish USP18 shows no conservation within IBB-1. Our results suggest that fish USP18 is a DUB cross-reactive with ubiquitin and ISG15. Furthermore, the IBB-1 region in fish USP18 has characteristics of ubiquitin-specific DUBs and lacks the two hydrophobic amino acids characteristic of IBB-1 of USP18.

Molecular modeling and interaction studies on several variants of mouse and human USP18 with ISG15 showed that the conclusions drawn from the structure also hold true for the human homologs. In contrast, a recent study has concluded that the mode of USP18-ISG15 interaction might differ between mouse and human proteins[51]. Our results further show that neither mouse nor human USP18 is able to catalyze deubiquitination *in vitro*, and we provide a molecular rationale for the remarkable specificity of USP18. However, two recent studies have provided evidence that USP18 is involved in deubiquitination of the TAK1–TAB1 complex[30] or NEMO[31], thereby inhibiting activation of NF-κB. These studies have suggested that USP18 influences the ubiquitination status of NEMO independently of its protease activity[31], but, in contrast, USP18 inhibits ubiquitination of the TAK1–TAB1 complex in a protease-dependent manner[30,31]. Our results clearly show that USP18 exhibits no reactivity toward ubiquitin *in vitro*, thereby indicating that the described inhibition of the NF-κB pathway by USP18 is an indirect effect, rather than being mediated by direct interaction between USP18 and ubiquitin.

In addition to ISG15, FAT10 is another member of the Ubl family that contains two Ubl domains. To date, no protease specific for FAT10 has been discovered. It is likely that such an enzyme exists, and it will be interesting to determine whether specificity is achieved via specific detection of a particular patch within one Ubl domain, as shown in this study for USP18 recognition of ISG15, or via contact with both Ubl domains.

Beyond its function as an ISG15 protease, USP18 is a major negative regulator of type I interferon signaling. This property is clearly independent of USP18's catalytic activity, because IFN signaling in mice selectively lacking the active site cysteine is unaffected[32]. Mutational studies have suggested that USP18 binds to the intracellular region of type I IFN receptor subunit IFNAR2 and outcompetes the downstream kinase JAK1, thereby abrogating IFN signaling[36]. The binding of primary signaling molecules to their cognate receptors in IFN signaling (JAK1 to IFNAR2 and Tyk2 to IFNAR1) has been suggested to be highly conserved[52]. In IFNAR2, the interaction region consists of two motifs termed Box 1 and Box 2, and Box 1 is critical for USP18 binding[36]. The hydrophobic nature of Box 1 and of the USP18-ISG15 interaction plane suggests that a similar mode of interaction might occur between USP18 and IFNAR2.

In summary, here we unraveled the molecular properties that determine the unique specificity of USP18. By identifying a distinct hydrophobic patch critical for ISG15-USP18 recognition, we showed that even small changes on the surface are sufficient to generate a highly specific enzyme capable of distinguishing between ubiquitin and the structurally related Ubl domain of ISG15.

## METHODS

Methods, including statements of data availability and any associated accession codes and references, are available in the online version of the paper.

*Note: Any Supplementary Information and Source Data files are available in the online version of the paper.*


### ACKNOWLEDGMENTS

We thank S. Ehrenfeld and A. Hausmann for assistance with cloning and expression of USP18 and D. el Atmioui for assistance with SPPS. The help of F. Garzoni in generating the insect-cell expression system is gratefully acknowledged. We thank C. Brancolini (University of Udine) and P. Boudinot (French National Institute for Agricultural Research) for providing materials. The expression-system work was financially supported by the European Community's Seventh Framework Programme (FP7/2007-2013) PCUBE. This work was further supported by grants from the Deutsche Forschungsgemeinschaft FR 1488/3-2 to G.F. and KN 590/3-2 and KN 590/1-3 to K.-P.K., and from the Dutch Technology Foundation (STW) to P.P.G. and H.O. This work was also supported by a grant from the European Research Council (ERC Grant agreement no. 281699 to H.O.). We thank the staff at beamlines X06DA and X06SA of the Swiss Light Source for excellent support. We thank the Diamond Light Source for access to beamlines I03 and I04-1 (MX9694, MX12090), which contributed to the results presented here. Finally, we thank the staff at beamlines P13 and P14 of PETRAIII for excellent support. The research leading to these results received funding from the European Community's Seventh Framework Programme (FP7/2007-2013) under grant agreement no. 283570 (for BioStruct-X).


### AUTHOR CONTRIBUTIONS

A.B., A.R., P.P.G., M.S.S. and P.S. expressed and purified proteins. A.B. and A.R. created variants and tested enzyme reactivity. A.B. crystallized the proteins and recorded X-ray diffraction data. G.F. performed data analysis. A.B. and G.F. performed model building and refinement. P.P.G. and K.F.W. created the covalent ISG15 and Ub probes and performed enzyme assays. A.B., S.H., A.R. and K.-P.K. performed cell culture experiments and immunoblot analysis. R.T. performed SPR analysis. A.B., H.O., K.-P.K. and G.F. designed experiments. A.B., K.-P.K. and G.F. wrote the manuscript.

### COMPETING FINANCIAL INTERESTS

The authors declare no competing financial interests.




1. Haas, A.L., Ahrens, P., Bright, P.M. & Ankel, H. Interferon induces a 15-kilodalton protein exhibiting marked homology to ubiquitin. *J. Biol. Chem.* **262**, 11315–11323 (1987).
2. Narasimhan, J. *et al.* Crystal structure of the interferon-induced ubiquitin-like protein ISG15. *J. Biol. Chem.* **280**, 27356–27365 (2005).
3. Yuan, W. & Krug, R.M. Influenza B virus NS1 protein inhibits conjugation of the interferon (IFN)-induced ubiquitin-like ISG15 protein. *EMBO J.* **20**, 362–371 (2001).
4. Kim, K.I., Giannakopoulos, N.V., Virgin, H.W. & Zhang, D.-E. Interferon-inducible ubiquitin E2, Ubc8, is a conjugating enzyme for protein ISGylation. *Mol. Cell. Biol.* **24**, 9592–9600 (2004).
5. Zhao, C. *et al.* The UbcH8 ubiquitin E2 enzyme is also the E2 enzyme for ISG15, an IFN-α/β-induced ubiquitin-like protein. *Proc. Natl. Acad. Sci. USA* **101**, 7578–7582 (2004).
6. Oudshoorn, D. *et al.* HERC6 is the main E3 ligase for global ISG15 conjugation in mouse cells. *PLoS One* **7**, e29870 (2012).
7. Ketscher, L., Basters, A., Prinz, M. & Knobeloch, K.-P. mHERC6 is the essential ISG15 E3 ligase in the murine system. *Biochem. Biophys. Res. Commun.* **417**, 135–140 (2012).
8. Wong, J.J.Y., Pung, Y.F., Sze, N.S.-K. & Chin, K.-C. HERC5 is an IFN-induced HECT-type E3 protein ligase that mediates type I IFN-induced ISGylation of protein targets. *Proc. Natl. Acad. Sci. USA* **103**, 10735–10740 (2006).
9. Dastur, A., Beaudenon, S., Kelley, M., Krug, R.M. & Huibregtse, J.M. Herc5, an interferon-induced HECT E3 enzyme, is required for conjugation of ISG15 in human cells. *J. Biol. Chem.* **281**, 4334–4338 (2006).
10. Zhao, C., Collins, M.N., Hsiang, T.-Y. & Krug, R.M. Interferon-induced ISG15 pathway: an ongoing virus-host battle. *Trends Microbiol.* **21**, 181–186 (2013).
11. Morales, D.J. & Lenschow, D.J. The antiviral activities of ISG15. *J. Mol. Biol.* **425**, 4995–5008 (2013).
12. Skaug, B. & Chen, Z.J. Emerging role of ISG15 in antiviral immunity. *Cell* **143**, 187–190 (2010).
13. Durfee, L.A., Lyon, N., Seo, K. & Huibregtse, J.M. The ISG15 conjugation system broadly targets newly synthesized proteins: implications for the antiviral function of ISG15. *Mol. Cell* **38**, 722–732 (2010).
14. Giannakopoulos, N.V. *et al.* Proteomic identification of proteins conjugated to ISG15 in mouse and human cells. *Biochem. Biophys. Res. Commun.* **336**, 496–506 (2005).
15. Zhao, C., Denison, C., Huibregtse, J.M., Gygi, S. & Krug, R.M. Human ISG15 conjugation targets both IFN-induced and constitutively expressed proteins functioning in diverse cellular pathways. *Proc. Natl. Acad. Sci. USA* **102**, 10200–10205 (2005).
16. Zou, W. *et al.* ISG15 modification of ubiquitin E2 Ubc13 disrupts its ability to form thioester bond with ubiquitin. *Biochem. Biophys. Res. Commun.* **336**, 61–68 (2005).
17. Takeuchi, T., Iwahara, S., Saeki, Y., Sasajima, H. & Yokosawa, H. Link between the ubiquitin conjugation system and the ISG15 conjugation system: ISG15 conjugation to the UbcH6 ubiquitin E2 enzyme. *J. Biochem.* **138**, 711–719 (2005).
18. Shi, H.X. *et al.* Positive regulation of interferon regulatory factor 3 activation by Herc5 via ISG15 modification. *Mol. Cell. Biol.* **30**, 2424–2436 (2010).
19. Lu, G. *et al.* ISG15 enhances the innate antiviral response by inhibition of IRF-3 degradation. *Cell. Mol. Biol.* **52**, 29–41 (2006).
20. D'Cunha, J., Knight, E. Jr., Haas, A.L., Truitt, R.L. & Borden, E.C. Immunoregulatory properties of ISG15, an interferon-induced cytokine. *Proc. Natl. Acad. Sci. USA* **93**, 211–215 (1996).
21. Bogunovic, D. *et al.* Mycobacterial disease and impaired IFN-γ immunity in humans with inherited ISG15 deficiency. *Science* **337**, 1684–1688 (2012).
22. Park, J.M. *et al.* Modification of PCNA by ISG15 plays a crucial role in termination of error-prone translesion DNA synthesis. *Mol. Cell* **54**, 626–638 (2014).
23. Forys, J.T. *et al.* ARF and p53 coordinate tumor suppression of an oncogenic IFN-β-STAT1-ISG15 signaling axis. *Cell Rep.* **7**, 514–526 (2014).
24. Sgorbissa, A. & Brancolini, C. IFNs, ISGylation and cancer: Cui prodest? *Cytokine Growth Factor Rev.* **23**, 307–314 (2012).
25. Komander, D., Clague, M.J. & Urbé, S. Breaking the chains: structure and function of the deubiquitinases. *Nat. Rev. Mol. Cell Biol.* **10**, 550–563 (2009).
26. Catic, A. *et al.* Screen for ISG15-crossreactive deubiquitinases. *PLoS One* **2**, e679 (2007).
27. Ye, Y. *et al.* Polyubiquitin binding and cross-reactivity in the USP domain deubiquitinase USP21. *EMBO Rep.* **12**, 350–357 (2011).
28. Basters, A. *et al.* Molecular characterization of ubiquitin-specific protease 18 reveals substrate specificity for interferon-stimulated gene 15. *FEBS J.* **281**, 1918–1928 (2014).
29. Malakhov, M.P., Malakhova, O.A., Kim, K.I., Ritchie, K.J. & Zhang, D.-E. UBP43 (USP18) specifically removes ISG15 from conjugated proteins. *J. Biol. Chem.* **277**, 9976–9981 (2002).
30. Liu, X. *et al.* USP18 inhibits NF-κB and NFAT activation during Th17 differentiation by deubiquitinating the TAK1-TAB1 complex. *J. Exp. Med.* **210**, 1575–1590 (2013).
31. Yang, Z. *et al.* USP18 negatively regulates NF-κB signaling by targeting TAK1 and NEMO for deubiquitination through distinct mechanisms. *Sci. Rep.* **5**, 12738 (2015).
32. Ketscher, L. *et al.* Selective inactivation of USP18 isopeptidase activity *in vivo* enhances ISG15 conjugation and viral resistance. *Proc. Natl. Acad. Sci. USA* **112**, 1577–1582 (2015).
33. Ketscher, L. & Knobeloch, K.P. ISG15 uncut: dissecting enzymatic and non-enzymatic functions of USP18 *in vivo*. *Cytokine* **76**, 569–571 (2015).
34. Rahnefeld, A. *et al.* Ubiquitin-like protein ISG15 (interferon-stimulated gene of 15 kDa) in host defense against heart failure in a mouse model of virus-induced cardiomyopathy. *Circulation* **130**, 1589–1600 (2014).
35. Goldmann, T. *et al.* USP18 lack in microglia causes destructive interferonopathy of the mouse brain. *EMBO J.* **34**, 1612–1629 (2015).
36. Malakhova, O.A. *et al.* UBP43 is a novel regulator of interferon signaling independent of its ISG15 isopeptidase activity. *EMBO J.* **25**, 2358–2367 (2006).
37. Meuwissen, M.E. *et al.* Human USP18 deficiency underlies type 1 interferonopathy leading to severe pseudo-TORCH syndrome. *J. Exp. Med.* **213**, 1163–1174 (2016).
38. Zhang, X. *et al.* Human intracellular ISG15 prevents interferon-α/β over-amplification and auto-inflammation. *Nature* **517**, 89–93 (2015).
39. Hu, M. *et al.* Crystal structure of a UBP-family deubiquitinating enzyme in isolation and in complex with ubiquitin aldehyde. *Cell* **111**, 1041–1054 (2002).
40. Faesen, A.C. *et al.* Mechanism of USP7/HAUSP activation by its C-terminal ubiquitin-like domain and allosteric regulation by GMP-synthetase. *Mol. Cell* **44**, 147–159 (2011).
41. Hu, M. *et al.* Structure and mechanisms of the proteasome-associated deubiquitinating enzyme USP14. *EMBO J.* **24**, 3747–3756 (2005).

42. Avvakumov, G.V. *et al.* Amino-terminal dimerization, NRDP1-rhodanese interaction, and inhibited catalytic domain conformation of the ubiquitin-specific protease 8 (USP8). *J. Biol. Chem.* **281**, 38061–38070 (2006).
43. Molland, K., Zhou, Q. & Mesecar, A.D.A. A 2.2 Å resolution structure of the USP7 catalytic domain in a new space group elaborates upon structural rearrangements resulting from ubiquitin binding. *Acta Crystallogr. F Struct. Biol. Commun.* **70**, 283–287 (2014).
44. Ekkebus, R. *et al.* On terminal alkynes that can react with active-site cysteine nucleophiles in proteases. *J. Am. Chem. Soc.* **135**, 2867–2870 (2013).
45. Békés, M. *et al.* Recognition of Lys48-linked di-ubiquitin and deubiquitinating activities of the SARS coronavirus papain-like protease. *Mol. Cell* **62**, 572–585 (2016).
46. Holm, L. & Rosenström, P. Dali server: conservation mapping in 3D. *Nucleic Acids Res.* **38**, W545–W549 (2010).
47. Borodovsky, A. *et al.* A novel active site-directed probe specific for deubiquitylating enzymes reveals proteasome association of USP14. *EMBO J.* **20**, 5187–5196 (2001).
48. Nakamura, N. & Hirose, S. Regulation of mitochondrial morphology by USP30, a deubiquitinating enzyme present in the mitochondrial outer membrane. *Mol. Biol. Cell* **19**, 1903–1911 (2008).
49. Huang, X. *et al.* Deubiquitinase USP37 is activated by CDK2 to antagonize APC(CDH1) and promote S phase entry. *Mol. Cell* **42**, 511–523 (2011).
50. Ratia, K., Kilianski, A., Baez-Santos, Y.M., Baker, S.C. & Mesecar, A. Structural basis for the ubiquitin-linkage specificity and deISGylating activity of SARS-CoV papain-like protease. *PLoS Pathog.* **10**, e1004113 (2014).
51. Speer, S.D. *et al.* ISG15 deficiency and increased viral resistance in humans but not mice. *Nat. Commun.* **7**, 11496 (2016).
52. Wallweber, H.J., Tam, C., Franke, Y., Starovasnik, M.A. & Lupardus, P.J. Structural basis of recognition of interferon-α receptor by tyrosine kinase 2. *Nat. Struct. Mol. Biol.* **21**, 443–448 (2014).

## ONLINE METHODS

**Cloning.** Sequences for all primers are listed in **Supplementary Table 1**. The vector pKL-His-3C-USP18 was generated as previously described[28]. Briefly, the cDNA of mouse USP18 encoding residues 46–368 was amplified from the vector pTriEx2-mUSP18 (ref. 32) with the primers BstBI-3C-USP18-for and HindIII-USP18-rev and cloned into the pKL vector[53]. In a second step, a hexahistidine ($His_6$) tag was introduced at the N terminus with the primers BstBI-His-3C-for and HindIII-USP18-rev. For generation of vectors encoding $His_6$-tagged USP18 variants, synthetic cDNAs comprising the respective cDNA flanked by BstBI and HindIII restriction sites were purchased from Life Technologies, digested with BstBI and HindIII and ligated into the pKL vector.

The sequence of human USP18 (hUSP18) cDNA encoding residues 16–372 was PCR amplified with the primers attB1-3C-hUSP18-for and attB2-hUSP18-rev and, as a template, the vector pCMV5a-hUSP18-Flag containing the full-length hUSP18 cDNA (kindly provided by C. Brancolini (University of Udine)). The PCR fragment was cloned into the pVL1393-$His_6$-GST vector (in-house modified) with the Gateway system (Invitrogen). The resulting sequence, encoding $His_6$-GST-3C-hUSP18(16–372), was sequence verified by an external service (BMR Genomics, Italy).

To generate the vector pTXB1-mISG15-C76S, the cDNA encoding amino acids 1–154 of mouse ISG15 was amplified from the vector pACE-ISG15-C76S[28] with the primers NdeI-ISG15-for and SpeI-ISG15-rev. The PCR product was digested with the restriction enzymes NdeI and SpeI and ligated into the pTXB1 vector. The vector pTXB1-hISG15-C78S was generated through cloning of a synthetic cDNA with codons optimized for expression in *Escherichia coli*, encoding residues 1–156 of human ISG15 with restriction sites NdeI and SpeI, into pTXB1 (New England BioLabs). The resulting vector contained a serine instead of a cysteine at position 78 of ISG15.

The expression vector for mouse ISG15 pACE-mISG15-C76S was generated as previously described[28]. Briefly, a synthetic cDNA encoding residues 1–155 with codons optimized for expression in *E. coli*, fused to an N-terminal $His_6$ tag and an HRV 3C protease–cleavage site, was cloned via NdeI and XhoI into the vector pACE. The coding sequence contained a serine instead of a cysteine at position 76. The expression vectors pACE-mISG15-C76S-W121 and pACE-mISG15-C76S-W121-P128G-H149V were likewise generated with synthetic cDNAs. In the coding sequences, Trp121 or Trp121, Pro128 and His149 were replaced by the corresponding residues of ubiquitin, respectively.

For cloning of pcDNA3.1-HA-ISG15-C, a synthetic cDNA encoding the C-terminal domain of mouse ISG15 (amino acid residues 77–155) in frame with an N-terminal HA tag was purchased from Life Technologies. The synthetic construct was digested with restriction enzymes NheI and BamHI and cloned into the vector pcDNA3.1 (Invitrogen). Plasmids encoding human Ube1l and human UbcH8 (ref. 9) as well as full-length mouse ISG15 and mouse Herc6 (ref. 7) were as previously described.

To generate an expression construct for USP18 of *D. rerio* (zebrafish), cDNA isolated from the intestine of the organism (kindly provided by P. Boudinot (French National Institute for Agricultural Research)) was used as a template for amplification with the primers KpnI-drUSP18-for and XhoI-drUSP18-rev. The PCR product was cloned into the vector pCR2.1 with a TA cloning kit (Life Technologies). The resulting vector was digested with the restriction enzymes KpnI and XhoI and cloned into the vector pTriEx2 (Novagen). The vector pTriEx2-drUSP18-C38A was generated with a QuikChange II kit (Stratagene) and the primers drUSP18-C38A-for and drUSP18-C38A-rev.

The vector pTriEx2-USP21cd encoding residues 197–565 of human USP21 was generated by amplification of USP21 cDNA from the vector Flag-HA-USP21 (Addgene) with the primers KpnI-USP21cd-for and XhoI-USP21cd-rev. The PCR product was digested with the restriction enzymes KpnI and XhoI and cloned into the vector pTriEx2 (Novagen).

**Protein expression and purification.** Mouse WT $His_6$-tagged USP18 as well as the mouse USP18 variants were expressed in *Sf*21 cells with the MultiBac system[53–56], as described in ref. 28. For large-scale expression, 200 ml of *Sf*21 cells at a density between 0.5 and $1 \times 10^6$ cells $ml^{-1}$ were infected with 200–600 µl of the respective virus. The cells were kept at the same density until proliferation arrest. Subsequently, expression of YFP was monitored every 24 h to determine the time point for cell harvesting. The cells were resuspended in buffer A (50 mM $Na_2HPO_4$, 500 mM NaCl and 4 mM DTT, pH 7.9) supplemented with 0.1% Tween 20, 5 mM $MgCl_2$ and traces of DNase, and lysed through two steps of freezing and thawing. The cleared lysate was applied to a 1-ml HisTrapFF column (GE Healthcare). The bound protein was eluted in buffer B (50 mM $Na_2HPO_4$, 500 mM NaCl, 500 mM imidazole and 4 mM DTT, pH 7.9).

$His_6$-GST-hUSP18(16–372) was expressed in *Sf*9 cells with a BaculoGold expression system (BD Biosciences) according to the manufacturer's standard protocol. The *Sf*9 cells were cotransfected with linearized BaculoGold DNA and pVL-$His_6$-GST-3C-USP18. The high-titer viral stock was generated by four rounds of amplification and was used for large-scale protein expression. For large-scale expression, 2 l of *Sf*9 cells at a density of $1.5 \times 10^6$ cells $ml^{-1}$ were infected with 15 ml of virus stock and harvested by centrifugation after 3 d of cultivation at 27 °C. The cells were lysed by homogenization (Emulsiflex, Avestin) in 150 ml of lysis buffer (50 mM $Na_2HPO_4$, 500 mM NaCl, 10% glycerol and 20 mM DTT, pH 8.0) supplemented with 20 µg $ml^{-1}$ DNase I, 1 mM $MgCl_2$, 0.01% Tween and protease-inhibitor cocktail. The lysate was cleared by centrifugation at 20,000*g* for 1 h at 4 °C, and the supernatant was applied to a 12-ml column of GST Sepharose 4FF (GE Healthcare). The column was washed with lysis buffer and equilibrated with 3C protease buffer (50 mM $Na_2HPO_4$, 500 mM NaCl, 10% glycerol, 2 mM DTT and 1 mM EDTA, pH 8.9). hUSP18 without a tag was obtained by 3C protease cleavage on a GST column at 4 °C overnight and elution in the same buffer. The protein was further purified by size-exclusion chromatography on a Superdex 200 (10/300) column (GE Healthcare) in a buffer containing 25 mM HEPES-NaOH, 500 mM NaCl, 10% glycerol and 2 mM DTT, pH 8.0. Mouse ISG15 variants were expressed and purified as described previously for ISG15 WT[28].

**Generation of ISG15-PA, ct-ISG15-PA and Ub-PA probes.** *ISG15-PA*. Mouse and human ISG15-PA were prepared with intein chemistry via a method similar to that previously reported[57]. Expression of mouse and human ISG15-intein fused to intein and chitin-binding domains was performed in *E. coli* BL21(DE3) cells with ZYP-5052 autoinduction medium[58] supplemented with 50 µg $ml^{-1}$ carbenicillin at 37 °C. After 3–4 h at an $OD_{600nm}$ of 0.6, the temperature was lowered to 18 °C, and the cells were allowed to grow an additional 16 h, after which they were harvested by centrifugation. The cell pellet from a 2.5-l culture was resuspended in 80 ml lysis buffer (50 mM HEPES, 100 mM sodium acetate, pH 6.5, with protease-inhibitor cocktail (Complete, Roche) and lysed by sonication. The lysate was clarified by centrifugation, and the supernatant was loaded onto a 30-ml chitin-bead column (New England BioLabs) at a flow rate of 0.5 ml $min^{-1}$. The column was washed with 120 ml lysis buffer, then with 60 ml lysis buffer containing 50 mM β-mercaptoethanesulfonic acid, sodium salt (MESNa). Another 30 ml of lysis buffer containing 50 mM MESNa was added to the beads, which were then incubated overnight at 37 °C. The ISG15-MESNa thioester was eluted with 25 ml lysis buffer. The combined fractions were concentrated by ultrafiltration and applied to a size-exclusion chromatography Superdex 75 (16/600) column equilibrated in 50 mM MES and 100 mM sodium acetate, pH 6.5, and eluted in the same buffer. Fractions containing ISG15-MESna were combined and concentrated by ultrafiltration (Millipore, Amicon Ultra-15 centrifugal filter units, 3,000-Da cutoff) to a concentration of 5 mg $ml^{-1}$. The ISG15-MESNa thioester was converted into the corresponding propargylamide (PA) by addition of propargylamine at a final concentration of 225 mM. LC–MS analysis indicated a complete conversion after 90 min. The mixture was acidified to pH 4.5 through the addition of acetic acid and was directly purified through RP-HPLC on a Waters HPLC system equipped with a Waters XBridge Prep C18 5-µm OBD column (30 × 150 mm). The column mobile phases were: A, MQ; B, $CH_3CN$; and C, 1% TFA in MQ. The flow rate was 37.5 ml $min^{-1}$, and a gradient of 20–60% B was applied with 10% C over 15 min. Pure fractions containing ISG15-PA were combined and lyophilized, thus yielding 22 mg of pure protein probe. The construct was dissolved in DMSO (10 mM) and reconstituted into buffer containing 50 mM MES and 100 mM NaCl, pH 6.5.

*Ac-ct-ISG15-PA*. The C-terminal domain of mouse ISG15 comprising residues 80–154 (ct-ISG15) was synthesized by solid-phase peptide chemistry (SPPS), via a method similar to that previously reported[59]. The peptide sequence Ac-LSILVR NERGHSNIYE VFLTQTVDTL KKKVSQREQV HEDQFWLSFE GRPMEDKELL GEYGLKPQCT VIKHLRLRG (corresponding to mouse ISG15 residues 80–154, with underlined residues indicating the positions where pseudoproline dipeptides were used) was synthesized in one linear automated (Prelude, Protein Technologies) Fmoc-based SPPS with a preloaded Fmoc-glycine-trityl-resin (TentaGel R Trt resin, RAPP Polymere, 0.19 mmol $g^{-1}$) on a 50-µmol scale.

12.5 µmol of the fully protected polypeptide was selectively cleaved from the resin by treatment with 1,1,1,3,3,3-hexafluoroisopropanol (20% (v/v) in DCM, 2 × 20 min.) after which all solvents were removed by evaporation under reduced pressure. The residue was dissolved in 2 ml DCM, and propargylamine (10 eq., 125 µmol, 8.0 µl), PyBOP (4 eq., 50 µmol, 26 mg) and triethylamine (4 eq., 50 µmol, 8.5 µl) were then added. After overnight stirring, the mixture was concentrated to dryness and coevaporated three times with 1,2-dichloroethane. The polypeptide was fully deprotected by treatment with TFA/$H_2O$/phenol/$iPr_3SiH$ (90.5:5:2.5:2, (v/v/v/v)) for 3 h. After the resin was washed with 3 × 1 ml TFA, the crude protein was precipitated with cold $Et_2O$/*n*-pentane (3:1 (v/v)). The precipitated protein was washed three times with $Et_2O$, and the pellet was dissolved in a mixture of $H_2O$/$CH_3CN$/AcOH (65:25:10 (v/v/v)) and finally lyophilized. The final product was purified through RP-HPLC on a Shimadzu LC-20AD/T equipped with a C8 Vydac column (Grace Davison Discovery Sciences). The column mobile phases were: A, 0.05% aq. TFA; B, 0.05% TFA in $CH_3CN$. The temperature was 40 °C, the flow rate was 5 ml $min^{-1}$, and a gradient of 25–60% B over 18 min was used. The pure product containing fractions were pooled and lyophilized. The Ac-ct-ISG15-PA probe was finally purified by size-exclusion chromatography with an NGC Chromatography System (Bio-Rad) equipped with a Superdex 75 (16/600) column (GE Healthcare) in a buffer containing 50 mM MES and 100 mM NaCl, pH 6.5, at a flow rate of 1 ml $min^{-1}$.

*Ub-PA*. Ub-PA was synthesized through a previously reported method[44].

**Enzyme kinetics and ISG15 FP and Ub FP assays.** The fluorescence polarization (FP) assays were performed in nonbinding-surface flat-bottom low-flange black 384-well plates (Corning) at room temperature in a buffer containing 50 mM Tris-HCl, pH 7.5, 2 mM DTT, 100 mM NaCl, 1 mg $ml^{-1}$ CHAPS and 0.5 mg $ml^{-1}$ bovine gamma globulin (BGG). Two-fold serial dilutions (200–0.4 nM) of the enzyme solutions (USP18 WT, $USP18^{IBB\text{-}1\text{-}USP7}$, $USP18^{IBB\text{-}2\text{-}USP7}$ and $USP18^{IBB\text{-}1\text{-}USP7\text{–}IBB\text{-}2\text{-}USP7}$) were made. 10 µl of each of the dilution steps was added to the empty wells of the plate. The reaction was started by addition of 10 µl of the ISG15-FP substrate or the Ub-FP substrate (200 nM final concentration)[28]. The fluorescence intensities in the *S* (parallel) and *P* (perpendicular) directions were recorded in intervals of 1 min on a BMG Labtech Pherastar plate reader (excitation, 540 nm; emission, 590 nm). From these *S* and *P* values, the FP values (in mP) were calculated by adjustment of the FP value (*L*) of the tracer molecule TAMRA-KG to 50 mP:

$$\text{Polarization (mP)} = \frac{S - (G \times P)}{S + (G \times P)} \times 1{,}000$$

where

$$G = \frac{\text{average } S}{\text{average } P} \times \frac{1 - L/1{,}000}{1 + L/1{,}000}$$

The kinetic parameters were determined with a fixed USP18 final concentration of 6 nM for USP18 WT, 500 nM for $USP18^{IBB\text{-}1\text{-}USP7}$, 6 nM for $USP18^{IBB\text{-}2\text{-}USP7}$ and 500 nM for $USP18^{IBB\text{-}1\text{-}USP7\text{–}IBB\text{-}2\text{-}USP7}$, and a serial dilution series of the substrate (0.2–5 µM). Kinetic data were collected in intervals of 90 s. From the obtained polarization values ($P_t$), the amount of processed substrate ($S_t$) was calculated with the following equation:

$$S_t = S_0 - S_0 \times \frac{P_t - P_{min}}{P_{max} - P_{min}}$$

where $P_t$ is the polarization measured (in mP); $P_{max}$ is the polarization of 100% unprocessed substrate (determined for every reagent at all used substrate concentrations); $P_{min}$ is the polarization of 100% processed substrate; and $S_0$ is the amount of substrate added to the reaction. From the obtained $P_t$ values, the values for initial velocities ($v_i$) were calculated, which were used to determine the Michaelis–Menten constants ($K_m$, $V_{max}$ and $k_{cat}$) by fitting the data according to the formula below (where $k_{cat} = V_{max}/[E]$). All experimental data were processed with Microsoft Excel and Prism 7.00 (GraphPad Software).

$$v_i = \frac{V_{max} \times S_0}{K_m + S_0}$$

**Analysis of the USP18-ISG15 interaction with surface plasmon resonance.** Surface plasmon resonance binding analysis was performed on a Biacore X100 machine (GE Healthcare). WT mouse USP18 and mouse USP18 variants were immobilized via the N-terminal $His_6$ tag on an NID200M Ni–NTA chip (XanTec Bioanalytics). Protein binding analysis was performed at 25 °C in 50 mM HEPES, 150 mM NaCl, 0.05 mM EDTA, 0.5 mM DTT and 0.01% P20, pH 7.5, with a flow rate of 20 µl $min^{-1}$. Stock solutions of mouse ISG15 and mouse ISG15 variants were diluted in running buffer. Binding traces were analyzed with BIAevaluation software (GE Healthcare) and fitted with a 1:1 binding model including a drift of the baseline.

**Reaction of USP18 and USP18 variants with PA probes.** USP18 WT and USP18 variants were diluted as pure proteins in 50 mM $Na_2HPO_4$, 500 mM NaCl and 10 mM DTT, pH 7.9, or in 50 mM Tris-HCl, 100 mM NaCl, 0.5 mg $ml^{-1}$ CHAPS and 5 mM DTT, pH 7.6, to a final concentration of 5 µM. Pure ISG15-PA, ct-ISG15-PA or Ub-PA probes were added at a 1:1 molar ratio and incubated for up to 60 min at room temperature.

For time-course experiments, samples were collected at 1 min, 5 min, and 40 min, and the reactions were stopped by addition of 4× loading buffer (250 mM Tris-Cl, pH 6.8, 40% (w/v) glycerol, 5% (w/v) SDS, bromophenol blue and 400 mM DTT). Complex formation was visualized by tricine SDS–PAGE[60].

**Reaction of USPs expressed in HEK 293T cells with PA probes.** HEK 293T cells were transfected with plasmids encoding full-length USP18 from different species (*M. musculus*, *Homo sapiens* and *D. rerio*) and the USP21 catalytic domain (residues 197–565) (*H. sapiens*) with Xtreme Gene (Roche) according to the manufacturer's instructions. The following variants of USP18 were obtained through gene synthesis: mouse $USP18^{IBB\text{-}1\text{-}USP7}$ with A138Q L142R H251Q; mouse $USP18^{IBB\text{-}2\text{-}USP7}$ with residues 256–263 (SARNSRTE) replaced by the corresponding residues 411–420 of USP7 (MYDPQTDQNI); mouse $USP18^{IBB\text{-}1\text{-}USP7\text{–}IBB\text{-}2\text{-}USP7}$ comprising both changes; human $USP18^{IBB\text{-}1\text{-}USP7}$ with A141Q L145R H255Q; human $USP18^{IBB\text{-}2\text{-}USP7}$ with residues 260–267 (SIRNSQTR) replaced by the corresponding residues 411–420 of USP7 (MYDPQTDQNI); and human $USP18^{IBB\text{-}1\text{-}USP7\text{–}IBB\text{-}2\text{-}USP7}$ comprising both changes. All proteins were expressed with an N-terminal S tag. Cells were lysed 48 h after transfection in 50 mM Tris-HCl, pH 7.4, 150 mM NaCl, 1 mM EDTA, 1% (v/v) Triton X-100 and 10 mM DTT. To monitor the reactivity and specificity of the different USPs, 10 µg of each lysate was combined with 1–2 µg of mISG15-PA, hISG15-PA or Ub-PA probes. The reaction mixtures in 50 mM $Na_2HPO_4$, 500 mM NaCl and 10 mM DTT, pH 7.9, were incubated for 2 h at 37 °C and stopped by addition of sample buffer and boiling. The samples were analyzed by immunoblotting with antibodies directed against the S tag (71549, Millipore) and GAPDH (AB2302, Millipore).

**Generation of ISGylated substrates and deISGylation assay.** USP18-deficient mouse embryonic fibroblasts were stimulated with 250 U/ml IFN-β for 24 h to induce ISGylation. To generate lysates with HA-ISG15- or HA-ct-ISG15-conjugated substrates, HEK 293T cells were transfected with vectors encoding hUbe1L, hUbcH8 and mHerc6 together with the plasmid encoding HA-ISG15 or HA-ct-ISG15. The cells were lysed in 50 mM Tris-HCl, pH 7.4, 150 mM NaCl, 1 mM EDTA and 1% (v/v) Triton X-100. 20 µg of the lysate was incubated with 20 µg of USP18 or the USP18 variants. The reactions were performed in 50 mM $Na_2HPO_4$, 500 mM NaCl, 10 mM DTT, pH 7.9, for 0 and 2 h at 37 °C. The samples were analyzed by immunoblotting with antibodies directed against ISG15 (ref. 61), HA (Y-11, Santa Cruz), β-actin (I-19, Santa Cruz) and GAPDH (AB2302, Millipore). Validation of the primary antibodies used is provided on the manufacturers' websites or in the corresponding reference citation.

**Generation of USP18–ISG15 complex for crystallization.** For crystallization, 4 mg of $His_6$-tagged USP18 was mixed with ISG15-PA at a 1:1 molar ratio and incubated for 30 min at 21 °C. The complex was purified by size-exclusion chromatography in 20 mM Tris-Cl, pH 7.9, 300 mM NaCl, 5 mM DTT and 0.1 mM EDTA with a Superdex 200 (16/600) column (GE Healthcare). The purified complex was supplemented with 50 mM DTT (final concentration) and directly used for crystallization.

**Crystallization.** Crystallization was performed in sitting-drop vapor-diffusion experiments at 20 °C. $His_6$-tagged USP18 was used at a concentration of 2.7 mg $ml^{-1}$ in 20 mM $Na_2HPO_4$, 300 mM NaCl and 50 mM DTT, pH 7.9, for crystallization. 300 nl of the protein was mixed with 300 nl crystallization solution and




doi:10.1038/nsmb.3371

equilibrated against 50 µl of the same solution. Initial spherulithes were obtained with 0.2 M $MgCl_2$, 0.1 M HEPES, pH 7.5, and 25% (w/v) PEG 3350 as a crystallization solution and were used to generate seed stocks. To this end, the spherulites were diluted and crushed in 50 µl crystallization solution. In subsequent crystallization trials, 300 nl protein was mixed with 200 nl crystallization solution and 100 nl seed stock, and crystals grew in 0.09 M succinate, pH 7.0, 13.5% (w/v) PEG 3350 and 10 mM KBr. Before vitrification in liquid nitrogen, the crystals were incubated for 1 min in crystallization solution supplemented with 20% (v/v) glycerol. The USP18–ISG15 complex was used at a concentration of 5 mg $ml^{-1}$ for crystallization. Spherulithes grew in 12.5% (w/v) PEG 1000, 12.5% (w/v) PEG 3350, 12.5% (v/v) MPD, 0.03 M $MgCl_2$, 0.03 M $CaCl_2$ and 0.1 M MES/imidazole, pH 6.5, and were used to generate seed stocks. The seed stock was added in further crystallization trials, and crystals were obtained with a crystallization solution with 12.5% (w/v) PEG 1000, 12.5% (w/v) PEG 3350, 12.5% (v/v) MPD, 0.03 M $NaNO_3$, 0.03 M $Na_2HPO_4$, 0.03 M $(NH_4)_2SO_4$ and 0.1 M MOPS-HEPES-NaOH, pH 7.5. The crystals were flash frozen in liquid nitrogen.

**Data collection, structure determination and refinement.** For USP18, data were collected at 100 K with a wavelength of 1.0 Å at beamline X06SA at the Swiss Light Source (Villigen, Switzerland) with a microfocus setup and a Mar225 CCD detector. Data for USP18–ISG15 were collected at 100 K with a wavelength of 1.0 Å at beamline X06DA, Swiss Light Source, equipped with a PILATUS 2M detector. All diffraction data were integrated with XDS[62]. The structure of unbound USP18 was solved by molecular replacement with Phaser[63] with USP7 (PDB 1NB8) as a search model. For the structure of the USP18–ISG15 complex, the structures of unbound USP18 and mouse ISG15 were used as search model in molecular-replacement trials with Phaser. Subsequent rounds of model building and refinement were carried out with Coot[64], Refmac5 (ref. 65) and phenix.refine[66]. Data collection and refinement statistics are given in **Table 1**. Figures of the structures were prepared with PyMOL[67].

**Structure and sequence analysis.** Multiple structural alignment was performed with the Dali server[46], with the coordinates of the USP18–ISG15 complex as a search model. The structures of human USPs were chosen from the list of structural neighbors, and the structure-based sequence alignment was visualized with Jalview[68]. The following structures were compared with USP18: USP7 (PDB 1NBF, chain B)[39], USP21 (PDB 2Y5B, chain A)[27], USP2 (PDB 2IBI, chain A), USP14 (PDB 2AYN, chain A)[41], USP8 (PDB 3N3K, chain A)[69], USP4 (PDB 2Y6E, chain B)[70], USP5 (PDB 3IHP, chain A)[71] and SARS CoV PLpro (PDB 5E6J, chain A)[45].

**Data availability.** Coordinates and structure factors for USP18 and the USP18–ISG15 complex have been deposited in the Protein Data Bank under accession codes PDB 5CHT and PDB 5CHV, respectively. Other data are available from the corresponding author upon reasonable request.


53. Bieniossek, C., Richmond, T.J. & Berger, I. MultiBac: multigene baculovirus-based eukaryotic protein complex production. *Curr. Protoc. Protein Sci.* **52**, 5.20 (2008).
54. Berger, I., Fitzgerald, D.J. & Richmond, T.J. Baculovirus expression system for heterologous multiprotein complexes. *Nat. Biotechnol.* **22**, 1583–1587 (2004).
55. Bieniossek, C., Imasaki, T., Takagi, Y. & Berger, I. MultiBac: expanding the research toolbox for multiprotein complexes. *Trends Biochem. Sci.* **37**, 49–57 (2012).
56. Bieniossek, C. *et al.* Automated unrestricted multigene recombineering for multiprotein complex production. *Nat. Methods* **6**, 447–450 (2009).
57. Hemelaar, J. *et al.* Specific and covalent targeting of conjugating and deconjugating enzymes of ubiquitin-like proteins. *Mol. Cell. Biol.* **24**, 84–95 (2004).
58. Studier, F.W. Protein production by auto-induction in high density shaking cultures. *Protein Expr. Purif.* **41**, 207–234 (2005).
59. El Oualid, F. *et al.* Chemical synthesis of ubiquitin, ubiquitin-based probes, and diubiquitin. *Angew. Chem. Int. Edn Engl.* **49**, 10149–10153 (2010).
60. Schägger, H. Tricine–SDS-PAGE. *Nat. Protoc.* **1**, 16–22 (2006).
61. Osiak, A., Utermöhlen, O., Niendorf, S., Horak, I. & Knobeloch, K.-P. ISG15, an interferon-stimulated ubiquitin-like protein, is not essential for STAT1 signaling and responses against vesicular stomatitis and lymphocytic choriomeningitis virus. *Mol. Cell. Biol.* **25**, 6338–6345 (2005).
62. Kabsch, W. XDS. *Acta Crystallogr. D Biol. Crystallogr.* **66**, 125–132 (2010).
63. McCoy, A.J. *et al.* Phaser crystallographic software. *J. Appl. Crystallogr.* **40**, 658–674 (2007).
64. Emsley, P., Lohkamp, B., Scott, W.G. & Cowtan, K. Features and development of Coot. *Acta Crystallogr. D Biol. Crystallogr.* **66**, 486–501 (2010).
65. Murshudov, G.N. *et al.* REFMAC5 for the refinement of macromolecular crystal structures. *Acta Crystallogr. D Biol. Crystallogr.* **67**, 355–367 (2011).
66. Adams, P.D. *et al. PHENIX*: a comprehensive Python-based system for macromolecular structure solution. *Acta Crystallogr. D Biol. Crystallogr.* **66**, 213–221 (2010).
67. The PyMOL Molecular Graphics System, Version 1.3r1 (Schrödinger, LLC, 2010).
68. Waterhouse, A.M., Procter, J.B., Martin, D.M.A., Clamp, M. & Barton, G.J. Jalview Version 2: a multiple sequence alignment editor and analysis workbench. *Bioinformatics* **25**, 1189–1191 (2009).
69. Ernst, A. *et al.* A strategy for modulation of enzymes in the ubiquitin system. *Science* **339**, 590–595 (2013).
70. Clerici, M., Luna-Vargas, M.P.A., Faesen, A.C. & Sixma, T.K. The DUSP-Ubl domain of USP4 enhances its catalytic efficiency by promoting ubiquitin exchange. *Nat. Commun.* **5**, 5399 (2014).
71. Avvakumov, G.V. *et al.* Two ZnF-UBP domains in isopeptidase T (USP5). *Biochemistry* **51**, 1188–1198 (2012).